AD-A178 881 CORRELATION OF ANALYTICAL CALCULATIONS FROM GRASP (GENERAL ROTORCRAFT AER... (U) ARMY AVIATION RESEARCH AND TECHNOLOGY ACTIVITY MOFFETT FIELD C... D L KUNZ ET AL. 1/1

UNCLASSIFIED 1987 F/G 20/4 NL

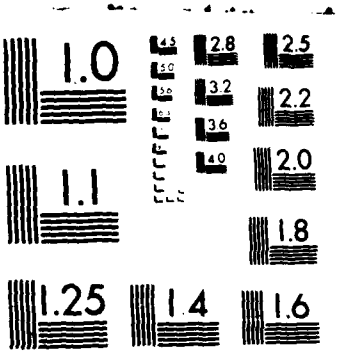

Correlation of Analytical Calculations from GRASP with Torsionally-Soft Rotor Data

Donald L. Kunz*
Aeroflightdynamics Directorate
U. S. Army Aviation Research and Technology Activity (AVSCOM)
Ames Research Center, Moffett Field, California
and
Dewey H. Hodges†
School of Aerospace Engineering
Georgia Institute of Technology
Atlanta, Georgia

Abstract

As a part of the continuing effort to develop and validate the General Rotorcraft Aeromechanical Stability Program (GRASP), a correlation study is presented to compare the frequency, moment, and stability data for a model-scale, torsionally-soft, helicopter rotor with GRASP numerical calculations. The hierarchical representation of the model rotor is discussed along with the calculations of the vacuum frequencies, the steady-state blade moments in air, and the aeroelastic stability. Correlation is generally quite good. The GRASP predictions of the first three vacuum flap frequencies are outstanding and the first vacuum lag and torsion frequencies correlate reasonably well with the experimental data. Consistently outstanding results are obtained for all of the steady blade moments. The calculations of stability data are in general as good as those made by other programs, but are not quite as good as anticipated.

Introduction

Since 1980, the General Rotorcraft Aeromechanical Stability Program (GRASP)[1] has been under development by a team at the Aeroflightdynamics Directorate. The purpose of developing this program is to provide a general-purpose tool for analyzing the aeroelastic stability of arbitrary rotorcraft configurations. To this end, the GRASP formulation is a hybrid of multibody methods and the traditional, finite-element method, combining the best features of each.[2,3] As with most multibody methods, GRASP allows large relative motions to occur between substructures, including rotations of one substructure relative to any other substructure (a necessity for any truly general rotorcraft program). As in traditional, finite-element formulations, GRASP analyzes structures that have been broken up into collections of elements. In addition, GRASP provides the capability for multilevel substructuring which allows the structure to be broken up into substructures, which in turn may be broken down into smaller substructures until the lowest-level substructures are elements. This substructuring capability facilitates the definition of local coordinate systems that are most convenient for the substructure.

Currently, GRASP supports three types of elements: the *aeroelastic beam*, the *rigid-body mass*, and the *air mass*. The *aeroelastic beam*, the main flexible-body element, is an elastic, variable-order, kinematically-nonlinear beam element that may be subjected to inertial, gravitational, and aerodynamic forces. In the derivation of the element static and dynamic equations[3,4] (which are never written out explicitly), it is assumed that the strains are small relative to unity. However, there are no small-angle assumptions nor are the kinematically-nonlinear effects truncated by an ordering scheme. The *rigid-body mass* element may undergo arbitrarily large displacements and rotations up to 180°, and is subject only to inertial and gravitational forces. The *air mass* element represents the flow of air through an axisymmetric rotor disk. The equations of motion are derived from blade-element/momentum theory for both the static[5] and dynamic[6] problems.

Since the completion of Version 1 of GRASP, intensive efforts are being made to validate the program by comparing its results with those of other programs and experimental data. As a part of this effort, correlations were made between GRASP and the data obtained in two model tests[7,8] involving a set of torsionally-soft rotor blades. This same data set was also used in the Integrated Technology Rotor (ITR) methodology assessment[9], in which many helicopter companies participated. One of the advantages of using this data set is that all of the elements currently implemented in GRASP must be used, as well as many of the constraints. While all of the elements and constraints have been tested and validated individually, this is the most comprehensive validation effort yet attempted using GRASP.

Experimental Model

The small-scale model used in both experiments[7,8] is a 37.851-in.-diameter, isolated, hingeless, two-bladed rotor. Although detailed information on the construction and

---

* Research Scientist, Member AHS.

† Professor, Member AHS

properties of the rotor system can be found in Ref. 7, a summary of that information is included in this paper to show the connection between the GRASP model and the physical configuration.

The rotor is mounted on a rigid test stand (Fig. 1) through which power and excitation are applied. To allow different values of precone, the rotor hub (Fig. 2) can be replaced with similar hubs. Outboard of the hub, the blade system can be conveniently divided up into three substructures: the pitch flexure, the root hardware, and the actual blade.

Pitch Flexure

Outboard of the hub is the pitch flexure (Fig. 2). Two flexures, one stiff and the other soft, were used in the experiments. Each flexure consists of four webs arranged in a partial-cruciform cross section (Fig. 3). The stiffness of each flexure is determined by the thicknesses of the webs.

Root Hardware

Between the flexure and the blade is the the root hardware. This hardware consists of the clamp ring, the droop wedge, and the blade root cuff. Like the hub, the droop wedge is interchangeable to permit the use of different values of droop angle. The blade root cuff serves as the attachment for the blade, which is bonded to the airfoil-shaped section of the cuff (Fig. 2).

Blade

The rotor blade has an NACA 0012 airfoil section, with neither twist nor taper. The blade construction consists of an unidirectional Kevlar spar and 0.003in.-thick, glass-fiber, cloth skin. The profile is maintained by a polyurethane foam core, with tantalum segments imbedded in the leading edge to control the center of gravity and the cross-sectional polar moment of inertia. Two sets of blades that have nearly identical properties were built for the experiment. However, the nonrotating lag frequency of each of the blades in Blade Set 1 is approximately 5% higher than the lag frequency of the blades in Blade Set 2.

GRASP Representation

In accordance with the modeling philosophy that GRASP fosters, the model rotor is subdivided into substructures that represent portions of the complete structure. Each substructure is then represented as a subsystem. The following subsections present the details of this numerical model.

Subsystem Hierarchy

The hierarchical organization of the GRASP system model is shown in Fig. 4. Each subsystem is represented by a triad which indicates the presence of a frame of reference. The triangles represent structural nodes and the diamonds represent air nodes. Lines connecting the symbols show the interconnections among the nodes.

Fourteen subsystems are used to model the experimental rotor system. Subsystem ITR represents the complete model, and has two children, AIR and HUB. Subsystem AIR is an *air mass* element that models the static air flow through the rotor disk. While dynamic inflow can be modelled using this type of element, it has not been implemented for this validation effort because the dynamic inflow equations implemented in GRASP are valid only for rotors having three or more blades. Subsystem HUB represents the entire physical structure of the rotor.

The three children of HUB are RING, FLEXURE, and ROOT. Subsystem RING is a *rigid-body mass* element that represents the clamp ring (Fig. 2). The pitch flexure (Fig. 2) is modelled by subsystem FLEXURE, which in turn has four children that represent the four flexure webs. The names of each web subsystem indicate the position (looking in towards the hub) of that web in the flexure: H for horizontal, V for vertical, L for left, R for right, T for top, and B for bottom. Each web is modelled by an *aeroelastic beam* element.

The entire structure outboard of the clamp ring is represented by subsystem ROOT. This susystem has two children, WEDGE and BLADE. Subsystem WEDGE is another *rigid-body mass* element, this time used to model the droop wedge (Fig. 2). The remaining structure is contained in subsystem BLADE, which also has two children, CUFF and BEAM. Subsystem CUFF is the *rigid-body mass* element that models the blade root cuff (Fig. 2) and BEAM is the *aeroelastic beam* element that models the rotor blade itself.

Subsystem Frames of Reference

Every subsystem in a GRASP model has a frame of reference associated with it. In the case of system-type subsystems, the frame positions and orientations relative to one another are specified in User Data. The capability of specifying frame orientations is used to great advantage in this model to define the precone, droop, and blade pitch angles for the blade (Fig. 5). While element-type subsystems also have frames associated with them (except for the *air mass*), their positions and orientations are fixed by the position and orientation of the element.

In subsystem ITR, the frame of reference is located at the hub center. The 1-axis of the dextral frame coordinate system is coincident with the rotor axis of rotation and the 3-axis points radially outward along the blade (Fig. 5). The angular velocity of the rotor is specified by making the entire model rotate relative to an inertial frame of reference. The reference frame for subsystem HUB is located at the interface between the hub and the flexure. Its orientation relative to the frame in ITR may be changed by a rotation about the 2-axis of the ITR frame. That angle of rotation is

calculations, the axial force was calculated to be approximately 387 lb, which is almost the same as that measured in Ref. 8 (approximately 390 lb).

The effects of structural damping are not included in GRASP. Therefore a constant value of structural damping must be added to the real part of the stability eigenvalues. For the stiff-flexure cases (Cases 1, 3, and 5) a value of -1.23 rad/sec is used. A value of -1.03 rad/sec is used for the soft-flexure cases. These approximate values are determined from the experimental values of damping for Cases 1 and 2 at 0 rpm (Ref. 7, Tables 10 and 14, respectively).

Correlation of GRASP with Experimental Data

Six configurations of the model rotor are used in this correlation effort. These configurations correspond to cases A/1 through A/6 in Ref. 9 and are referred to as Cases 1 through 6, respectively, in this paper. The variable properties that were investigated are the stiffness of the pitch flexure, precone angle, and droop angle. Table 1 gives a summary of the characteristics of each case.

Vacuum Frequencies

Tables 2–7 summarize the correlation of GRASP calculations with the experiment reported in Ref. 8. The modal frequencies are given in rad/sec for the five modes measured. Note that there are two frequencies given for the experiment. The first frequency is that measured for the blade in Blade Set 2 designated Blade 8, and the second is for the blade designated 5. The correlation is outstanding for most of the modes and cases. In general, the most troublesome frequencies to predict are those for the lag and torsion modes. However, even for these modes, the GRASP calculations were usually within 6% of the experimental values. One exception is in Case 4 where the torsion frequency is 9.5% too low at 0 rpm, and 18.6% too high at 1000 rpm. Also, in Case 6, the torsion frequency is 7.0% too high at 1000 rpm.

Upon closer examination of the tables, it can be seen that at 0 rpm the flapping frequencies are relatively insensitive to the configuration. However, a very slight decrease can be detected when the soft flexure is installed. In Case 2, the GRASP calculations indicate a much more pronounced decrease in the third flap frequency at 0 rpm than that measured experimentally. Note that the third flap frequency for GRASP in Case 3 is missing. The algorithm that GRASP uses to calculate the eigenvalues found four of them, but failed to converge on the fifth.

For the lag mode, it can be seen that the GRASP frequencies are consistently higher than the experimental frequencies at 0 rpm in the stiff-flexure cases (Cases 1, 3, and 5), but are very close at 1000 rpm. In the soft-flexure cases, the GRASP frequencies show good correlation at 0 rpm (except perhaps in Case 6), but at 1000 rpm are too high. This is particularly evident in Case 4, where the measured lag frequency is smaller at 1000 rpm than at 0 rpm. GRASP calculations for that case show that the lag frequencies for those two rotor speeds should be approximately equal.

Interpretation of the correlation of the torsion frequencies predicted by GRASP with the experimental data is somewhat more difficult than for the flap and lag frequencies. First, for 6 of the 12 data points, there is significant scatter in the data. Also, the consistent trends that were discussed previously for the other modes do not appear here. It is apparent that at 0 rpm the GRASP torsion frequencies are higher than the measured frequencies for all of the stiff-flexure cases. For the soft-flexure cases, the GRASP frequencies are lower than the measured frequencies for Cases 2 and 4 at 0 rpm, but are very close for Case 6. At 1000 rpm, the GRASP torsion frequencies are high for the soft-flexure, preconed case (Case 4) and the soft-flexure, drooped case (Case 6). No trend can be discerned for the stiff-flexure cases.

The discrepancies between the measured and calculated frequencies are apparently a result of the way that GRASP models the pitch flexure. The webs in the flexure are really much more plate-like than beam-like. By treating the webs as beams, some aspects of their elastic properties may be being modeled incorrectly. This idea is supported by the results for the stiff flexures, which were considerably better than those for the soft flexures. In addition, axial force calculations for the webs in Cases 3 through 6 show that at 1000 rpm the lower flap web (WEBVB) is in compression . This is not a problem for the stiff flexures, but for the the soft flexures the compressive forces may exceed the buckling loads for that web.

Steady-State Moments

The steady-state moments calculated by GRASP are compared to the experimental data in Figs. 6–11. In general, the correlation is excellent. For some cases, the GRASP results and the experimental data for the lag and flap moments (M_1 and M_2, respectively) diverge somewhat at very high pitch angles. Although this discrepancy is small, note that the calculated results at the higher pitch angles are consistently smaller in magnitude than the data. This may indicate that the equations for the nonlinear lift and drag coefficients are not appropriate for that range of pitch angles.

When comparisons are made between theoretical calculations and experimental data, it is not usually a sound practice to blame discrepancies on the experimental data (especially high-quality, well-documented data like this). However, the data for Case 1 (Fig. 6) warrants critical examination for the following reasons. (1) First, the data point at 0° pitch in the lag moment plot is clearly at variance with both the numerical results and the other experimental data points. (2) Next, consider the flap moments in Figs. 6 and 7. Except for the experimental data in Fig. 6, the GRASP results in both figures and the experimental data in Fig. 7 cross the M_2 axis just below the origin. Since

the precone angle. In addition to having its frame position and orientation defined relative to the ITR frame, subsystem HUB (and consequently all of its children) is replicated to account for the two blades in the rotor.

The frame in subsystem FLEXURE is colocated with the HUB frame. Changes in blade pitch angle are implemented by rotating the frame in subsystem ROOT about the 3-axis of the HUB frame (Fig. 5). The ROOT frame is located at the inboard face of the droop wedge. The frame for subsystem BLADE is then located at the interface between the droop wedge and the blade root cuff, and its orientation relative to the ROOT frame depends on the droop angle (a rotation about the 2-axis).

Subsystem Nodes

In a GRASP model, material points on a structure are designated by *structural nodes*. For this model, three *structural nodes* are defined. Node FLEXROOT, defined in subsystem HUB, is located at the inboard face of the flexure, and is coincident with the HUB frame. In subsystem BLADE, node BLDROOT is defined. It is located at the root of the blade, and is therefore offset from the BLADE frame by 1.500 in. in the 3-direction (Fig. 5). Node BLDTIP, which is also defined in subsystem BLADE, is located at the blade tip and is offset 35.750 in. (in the 3-direction) from the BLADE frame.

To introduce the generalized coordinates necessary to model the steady-state air flow through the rotor, an *air node* (INFLOW) is defined in subsystem ITR. Node INFLOW is coincident with the ITR frame and rotates with it. Generally, air nodes are not defined in rotating coordinate systems, but since only static inflow degrees of freedom are being used in this model, there is no problem with allowing the air node to rotate.

Element Properties

In the preceding discussion of the experimental model, the blade system was divided into three substructures. The GRASP model element properties are described using the same divisions. The basic properties of the blade system, as measured for the experimental studies, are given in Table 1 of Ref. 8.

Pitch Flexure. Since only the soft-pitch-flexure properties are tabulated in the literature[7,8] (for the purposes of the experiment, the stiff flexure is assumed to be rigid), the inertial and elastic properties of both flexures are calculated. Instead of trying to calculate equivalent, single-beam approximations for both the stiff and soft flexures, each of the webs (WEBHI, WEBHR, WEBVB, and WEBVT) is modeled as an *aeroelastic beam*.

The area and moments of inertia for each web are calculated from the standard formulae for rectangular cross-sections. Values of the torsion inertia for the webs are obtained from Ref. 10. Note that this approach to modeling the pitch flexure also introduces a degree of approximation, since the webs are really shaped more like plates or short, deep beams rather than like slender beams.

Root Hardware. Because the blade pitch angle changes occur at the 1.726-in. radial station and droop angle changes occur at the 2.101-in. radial station, the root hardware is divided into three *rigid-body mass* elements: RING, WEDGE, and CUFF. To calculate the inertia and stiffness properties of these elements, the data in Table 1 of Ref. 8 are used. It is necessary to separately calculate the mass, torsion inertia, and center of gravity for each element.

Blade. Most of the blade physical properties are also taken from Table 1 of Ref. 8. However, it is necessary to calculate the axial stiffness and the first area moment of inertia of axial stiffness about the blade cross-section 1-axis (Fig. 5) in order to account for the 0.0884-in. tension axis offset. Also, the first area moment of mass about the 1-axis is included to account for the -0.0034-in. offset of the center of gravity. To improve the accuracy of the calculations, internal degrees of freedom are included for bending, extension, and torsion. For bending, 10th-order polynomials are specified, while 8th-order polynomials are used for extension and torsion. This results in the beam having 36 degrees of freedom rather than the normal 12 degrees of freedom.

The only blade aerodynamic properties required for this model are the chord width (3.400 in.), the offset of the aerodynamic center from the elastic axis (0.0068 in.), and the drag, lift, and moment coefficients. The nonlinear expressions for the aerodynamic drag and lift coefficients of the NACA 0012 airfoil section that are used for the blade are taken from Eq. (21) of Ref. 11.

$$c_d = 0.01 + 11.1|\alpha|^3$$
$$c_l = 6\alpha - 10\alpha|\alpha|$$

where α is the blade section angle of attack. The moment coefficent is assumed to be zero for all α.

Postprocessing of Results

For this correlation effort, very little postprocessing is required for either the experimental data or the results from GRASP. The only change made to the experimental data is that frequencies are converted from Hz to rad/sec. Otherwise, the data are copied or plotted directly from the experiment run logs.

Since GRASP calculates the steady-state moments at the elastic axis, it is necessary in the calculation of the lag moment to add the the product of the axial force (calculated by GRASP) and the tension axis offset to the lag moment at the elastic axis. Since the contributions from the axial force may make up a significant part of the total lag moment (approximately 34 in-lb), the axial force calculation takes on great importance. As part of the vacuum

Cases 1 and 2 are identical except for the flexure stiffness, it is likely that the flap moments measured for Case 1 contain an offset of approximately 10 in-lb. (3) Finally, experimental data for the torsion moment M_3 in Fig. 6 shows that the moment values at negative pitch angles are all negative. When these results are compared to the analogous soft-flexure case (Fig. 7), the torsion moment is shown to monotonically increase with decreasing pitch angle.

Apart from the anomalies in the data noted above, the only discrepancy in the correlation of the steady-state moments involves the torsion moment M_3. For all of the cases, the slope of the torsion moment measured in the experiment and that calculated by GRASP are different. However, this difference in slope is very consistent for all six cases. One possible explanation is that the aerodynamic moment coefficient for the airfoil section is not really zero, as was assumed in the GRASP model. Another possibility is that a component of the centrifugal force acting at the tension axis and in the plane of the deformed-blade cross-section produces an additional torsion moment.

Aeroelastic Stability

The correlation of the GRASP aeroelastic stability calculations with the experimental data from Ref. 7 is presented in Figs. 12–17. These figures also present the results from the program PFLT, which is based on the analysis described in Ref. 12. In Refs. 7 and 9, the damping calculations from PFLT showed good correlation with the data from the experiment. PFLT also performed very well in comparison with other analyses. In both of those correlation efforts, the blade structural damping was calculated internally by PFLT. To get a truer comparison with GRASP in this study, the PFLT internal structural damping was set to zero, and the constant values discussed above were used. This modification to PFLT was not too significant since the values that it calculates for structural damping are nearly constant with pitch angle.

Case 1: Stiff flexure, no precone or droop. The comparison of the Case 1 results from GRASP and PFLT, along with the test data, is displayed in Fig. 12. Both GRASP and PFLT correlate well with the measured frequencies, the discrepancies being less than 2%. At low pitch angles, the damping results from both analyses correlate well with the data, but neither correlates well at the higher angles. Note that PFLT is symmetric in pitch angle, while GRASP is not. This occurs because PFLT does not contain gravitational effects.

Case 2: Soft flexure, no precone or droop. The Case 2 correlation is shown in Fig. 13. Both GRASP and PFLT predict frequencies greater than the measured values, but the GRASP predictions are much closer (4% discrepancy for GRASP, 9.5% for PFLT). This characteristic of the analyses is repeated for all of the other soft-pitch-flexure cases (Cases 4 and 6). The GRASP frequency and damping results for this case also clearly show the effect of the nonlinear aerodynamic section coefficents. At the higher pitch angles, the frequency rise tends to flatten out while the damping flattens out and then starts to decrease.

Case 3: Stiff flexure, 5° precone, no droop. Like Case 1, the frequency results for Case 3 (Fig. 14) show the discrepancies among GRASP, PFLT, and the measured data to be small. This observation is consistent with the facts that PFLT contains no lag flexibility in its pitch flexure representation and the stiff flexure is nearly rigid. The damping results for this case show both GRASP and PFLT overshooting the minimum damping measured by the experiment. The minimum damping calculated by GRASP is smaller than that calculated by PFLT.

Case 4: Soft flexure, 5° precone, no droop. Case 4 (Fig. 15) is the most challenging case of this set. GRASP results are within 3% of the measured frequencies, but are not nearly as close for damping. On the other hand, PFLT does quite well for damping, but calculates frequencies that are more than 8% too high. The discrepancies between PFLT and the frequency data can again be attributed to the lack of flexibility in PFLT's representation of the pitch flexure. However, it is not clear what causes the discrepancies between GRASP and the damping data. Attempts were made to isolate the cause by modifying the lift and drag coefficients, but these attempts had little effect on the results.

Case 5: Stiff flexure, no precone, -5° droop. The frequency plot for Case 5 (Fig. 16) is interesting because it clearly shows the effect of the 5% difference in lag stiffness betweeen Blade Sets 1 and 2. The results from PFLT correlate better with the Blade Set 1 data, whereas the GRASP results correlate better with the Blade Set 2 data. Since the input data for both PFLT and GRASP were formulated from the properties of Blade Set 2 and it has already been shown that PFLT will always predict frequencies that are too high, the excellent correlation of PFLT results specifically with the Blade Set 1 data must be considered somewhat fortuitous.

As in Case 3, both GRASP and PFLT predict similar damping values but overshoot the minimum damping. The effect of the nonlinear lift and drag curves used by GRASP is evident at the higher pitch angles. Also, the damping values (as well as the frequencies) calculated by both GRASP and PFLT for this case are nearly identical to the results calculated for Case 3. This confirms the observation made in Ref. 7 that precone and negative droop are equivalent for the case of a stiff pitch flexure.

Case 6: Soft flexure, no precone, -5° droop. The frequency correlation for Case 6 (Fig. 17) follows the pattern of Cases 2 and 4. GRASP is slightly high in its frequency predictions and PFLT is considerably higher. Both GRASP and PFLT do reasonably well in their damping predictions at the lower pitch angles, but the quality degrades as the pitch angles increase.

Concluding Remarks

In general, the correlation of GRASP results with experimental data for vacuum frequencies, steady-state moments, and aeroelastic stability is very encouraging. The ability of GRASP to accurately predict the vacuum flap frequencies for all six configurations is outstanding. GRASP also performed very well in predicting the vacuum lag frequencies for the stiff-flexure cases. The discrepancies between the GRASP calculations and the measured lag and torsion frequencies for the soft-flexure cases can most likely be attributed to the modeling of the pitch flexure. Better correlation might be obtained if there were a plate element available that could model the webs more accurately.

The lag and flap moments calculated by GRASP also show outstanding correlation with the experimental data. Although the GRASP torsion moments are less accurate than the bending moments, the results are still quite good. However, it would be worthwhile to investigate means to improve the correlation.

The frequency predictions for aeroelastic stability generally follow the same trends as the vacuum lag frequencies. Therefore, improvements made in the vacuum calculations would have a similar effect on the frequencies in air. The major area of concern in the stability predictions is the discrepancy between the GRASP results and the experimental data for the aeroelastic damping of preconed rotors (Cases 3 and 4). Considerable effort needs to be made to resolve the differences between GRASP and PFLT. This will probably include a comparison of the aerodynamic equations for both analyses and a search for any significant differences in the structural representations.

Although GRASP has not yet reached maturity, it has already begun to show remarkable promise in its ability to handle complex rotor configurations. In this effort, the first extensive test of its capabilities, GRASP produced consistently good and often outstanding results without modifications to its input data using *ad hoc* correction factors. In addition, its results compared favorably to older, more mature programs (Ref. 9) which do not contain the generality inherent in GRASP.

Acknowledgements

The authors gratefully acknowledge the assistance of Mr. David L. Sharpe of the Aeroflightdynamics Directorate in providing access to his notes on the design of the blade components and the original test data.

Dr. Hodges' contributions to the writing of this paper were supported by Grant E-16-697 from the Georgia Tech Research Center.

References

[1]Hodges, D. H., Hopkins, A. S., Kunz, D. L., and Hinnant, H. E., "Introduction to GRASP - General Rotorcraft Aeromechanical Stability Program - A Modern Approach to Rotorcraft Modeling," Proceedings of the 42nd Annual Forum of the American Helicopter Society, Washington, D.C., June 2–4, 1986.

[2]Hopkins, A. S., and Likins, P. W., "Analysis of Structures with Rotating, Flexible Substructures," Proceedings of the AIAA Dynamics Specialists Conference, AIAA Paper No. 87-0951-CP, Monterey, Calif., Apr. 9–10, 1987.

[3]Hodges, D. H., Hopkins, A. S., and Kunz, D. L., "Analysis of Structures with Rotating, Flexible Substructures Applied to Rotorcraft Aeroelasticity in GRASP," Proceedings of the AIAA Dynamics Specialists Conference, Paper No. AIAA-87-0952-CP, Monterey, Calif., Apr. 9–10, 1987.

[4]Hodges, D. H., "Nonlinear Equations of Motion for Dynamics of Pretwisted Beams Undergoing Small Strains and Large Rotations," NASA TP-2470 (AVSCOM TR-84-A-5), May 1985.

[5]Gessow, A. and Myers, G. C., *Aerodynamics of the Helicopter*, Frederick Unger Publishing Company, New York, 1967, pp. 67–68.

[6]Pitt, D. M. and Peters, D. A., "Theoretical Predictions of Dynamic Inflow Derivatives," *Vertica*, 5, (1), Mar. 1981, pp. 21–34.

[7]Sharpe, D. L., "An Experimental Investigation of the Flap-Lag-Torsion Aeroelastic Stability of a Small-Scale Hingeless Helicopter Rotor in Hover," NASA TP-2546 (AVSCOM TR-85-A-9), Jan. 1986.

[8]Srinivasan, A. V., Cutts, D. G., and Shu, H. T., "An Experimental Investigation of the Structural Dynamics of a Torsionally Soft Rotor in a Vacuum," NASA CR-177418, July 1986.

[9]Sharpe, D. L., "A Comparison of Theory and Experiment for Aeroelastic Stability of a Hingeless Rotor Model in Hover," Proceedings of the ITR Methodology Assessment Workshop, Ames Research Center, Moffett Field, Calif., June 21–22, 1983.

[10]Roark, R. J. and Young, W. C., *Formulas for Stress and Strain*, 5th Ed., McGraw-Hill Book Co., Inc., 1975, pp. 300–303.

[11]Ormiston, R. A. and Bousman, W. G., "A Study of Stall-Induced Flap-Lag Instability of Hingeless Rotors," Proceedings of the 29th Annual Forum of the American Helicopter Society, Preprint No. 730, Washington, D.C., May 1973.

[12]Hodges, D. H., "Nonlinear Equations of Motion for Cantilever Rotor Blades in Hover With Pitch-Link Flexibility,Twist, Precone, Droop, Sweep, Torque Offset, and Blade Root Offset," NASA TM X-73,112, May 1976.

Table 1 Rotor blade configurations.

Case	Flexure	Precone	Droop	Blade Pitch
1	Stiff	0°	0°	-8° to 10°
2	Soft	0°	0°	-12° to 12°
3	Stiff	5°	0°	-2° to 10°
4	Soft	5°	0°	-2° to 12°
5	Stiff	0°	-5°	-2° to 14°
6	Soft	0°	-5°	0° to 12°

Table 2 Vacuum frequencies for Case 1 (stiff flexure, no precone or droop, 0° pitch).

Mode		0 rpm	1000 rpm
1st Flap	GRASP	32.53	122.90
	Ref. 8	32.74	122.65
		33.62	123.09
2nd Flap	GRASP	203.79	349.33
	Ref. 8	202.13	351.48
		207.35	351.73
3rd Flap	GRASP	570.45	738.83
	Ref. 8	576.80	737.46
		570.58	738.71
1st Lag	GRASP	143.77	156.57
	Ref. 8	150.92	157.65
		150.98	158.08
1st Torsion	GRASP	284.10	309.67
	Ref. 8	274.01	301.15
		273.26	316.30

Table 3 Vacuum frequencies for Case 2 (soft flexure, no precone or droop, 0° pitch).

Mode		0 rpm	1000 rpm
1st Flap	GRASP	32.46	122.65
	Ref. 8	32.61	121.71
		33.62	121.27
2nd Flap	GRASP	203.10	348.26
	Ref. 8	202.32	343.82
		210.05	345.76
3rd Flap	GRASP	559.44	735.53
	Ref. 8	569.13	727.78
		561.28	727.28
1st Lag	GRASP	138.05	150.79
	Ref. 8	138.42	141.43
		138.54	141.31
1st Torsion	GRASP	229.49	273.26
	Ref. 8	238.51	277.09
		237.50	315.42

Table 4 Vacuum frequencies for Case 3 (stiff flexure, 5° precone, no droop, 0° pitch).

Mode		0 rpm	1000 rpm
1st Flap	GRASP	32.51	122.85
	Ref. 8	32.61	127.67
		33.87	121.89
2nd Flap	GRASP	203.77	349.29
	Ref. 8	202.82	346.33
		207.35	347.46
3rd Flap	GRASP	570.42	-
	Ref. 8	569.13	733.37
		568.44	731.11
1st Lag	GRASP	143.77	152.58
	Ref. 8	149.41	153.94
		148.91	153.62
1st Torsion	GRASP	284.10	313.19
	Ref. 8	277.34	305.61
		315.16	317.87

Table 5 Vacuum frequencies for Case 4 (soft flexure, 5° precone, no droop, 0° pitch).

Mode		0 rpm	1000 rpm
1st Flap	GRASP	32.43	122.60
	Ref. 8	-	121.45
		-	122.46
2nd Flap	GRASP	203.08	348.22
	Ref. 8	202.13	344.51
		206.65	341.93
3rd Flap	GRASP	567.81	735.58
	Ref. 8	569.82	734.57
		561.09	735.13
1st Lag	GRASP	138.05	138.08
	Ref. 8	137.66	134.15
		138.23	134.02
1st Torsion	GRASP	229.47	288.10
	Ref. 8	245.11	242.91
		261.76	242.85

Table 6 Vacuum frequencies for Case 5 (stiff flexure, no precone, -5° droop, 0° pitch).

Mode		0 rpm	950 rpm
1st Flap	GRASP	32.51	117.32
	Ref. 8	32.74	–
		32.74	–
2nd Flap	GRASP	203.77	337.96
	Ref. 8	203.32	–
		202.51	–
3rd Flap	GRASP	570.42	724.39
	Ref. 8	573.72	718.42
		570.64	721.12
1st Lag	GRASP	143.76	153.81
	Ref. 8	150.23	153.81
		150.67	153.56
1st Torsion	GRASP	284.10	310.97
	Ref. 8	277.97	337.66
		279.10	314.85

Table 7 Vacuum frequencies for Case 6 (soft flexure, no precone, -5° droop, 0° pitch).

Mode		0 rpm	1000 rpm
1st Flap	GRASP	32.43	122.62
	Ref. 8	32.55	122.52
		33.62	123.21
2nd Flap	GRASP	203.08	348.23
	Ref. 8	201.38	349.22
		205.46	349.41
3rd Flap	GRASP	567.81	735.62
	Ref. 8	566.93	734.19
		568.44	732.81
1st Lag	GRASP	118.65	145.41
	Ref. 8	125.54	139.80
		126.17	140.68
1st Torsion	GRASP	238.79	273.39
	Ref. 8	237.19	255.29
		237.50	255.54

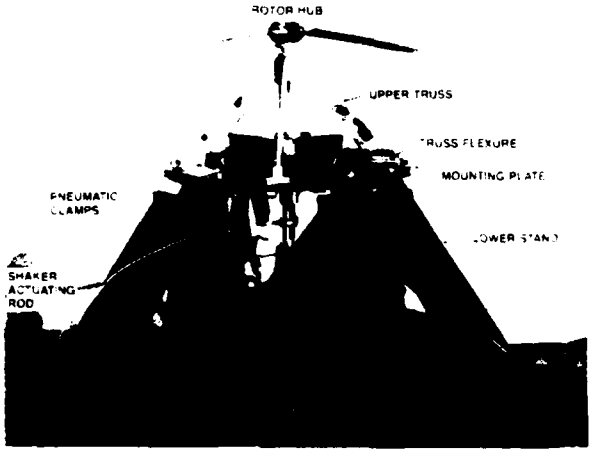

Fig. 1 Experimental rotor and test stand.

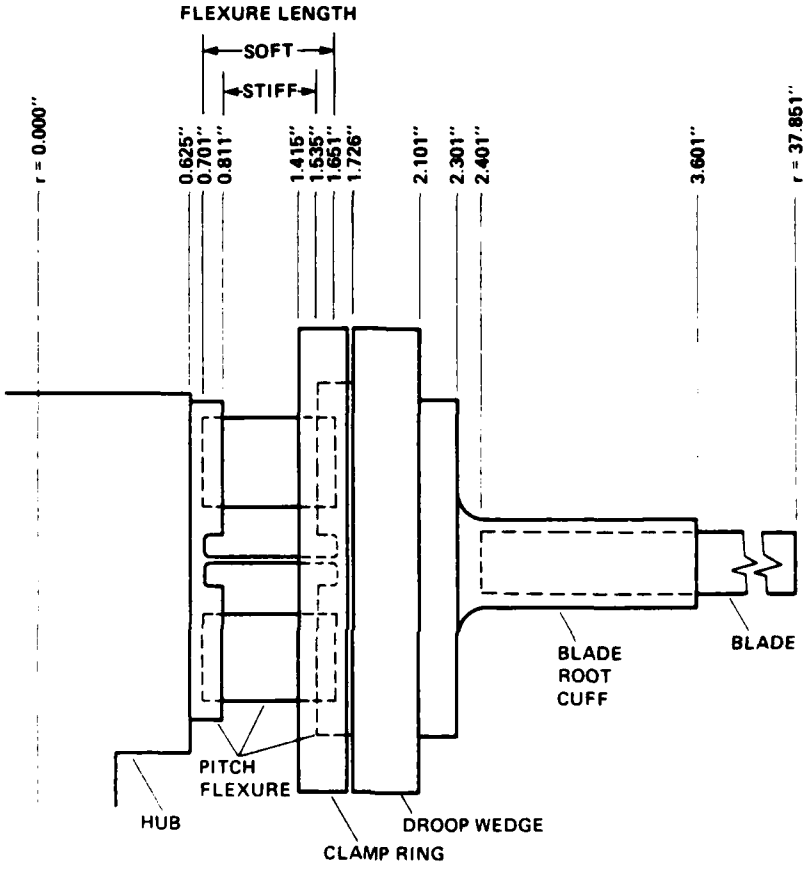

Fig. 2 Blade system components.

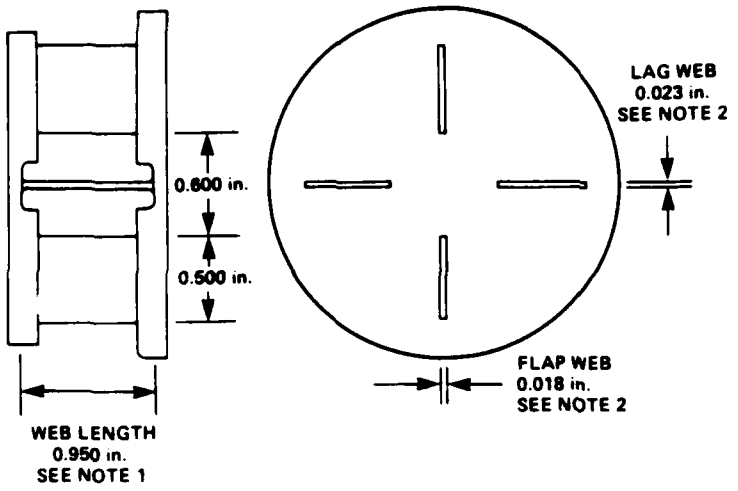

NOTE 1: SOFT PITCH FLEXURE ONLY
STIFF PITCH FLEXURE WEBS 0.724 in.

NOTE 2: SOFT PITCH FLEXURE ONLY
ALL STIFF PITCH FLEXURE WEBS 0.200 in.

Fig. 3 Pitch flexure cross-section.

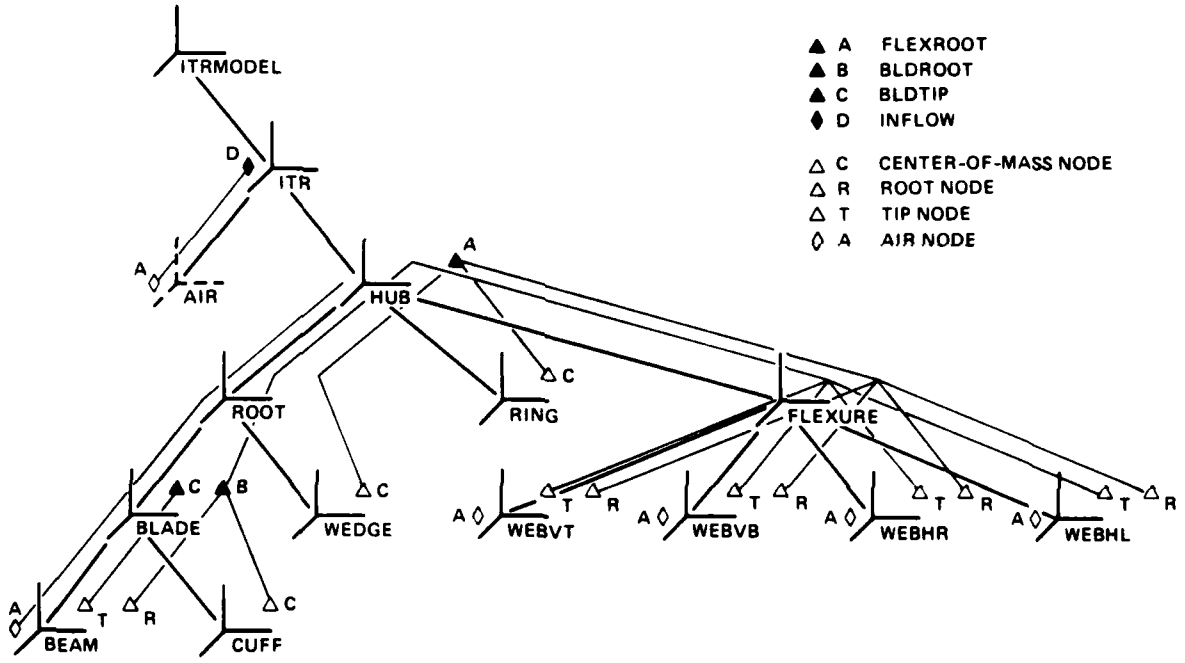

Fig. 4 GRASP model hierarchy.

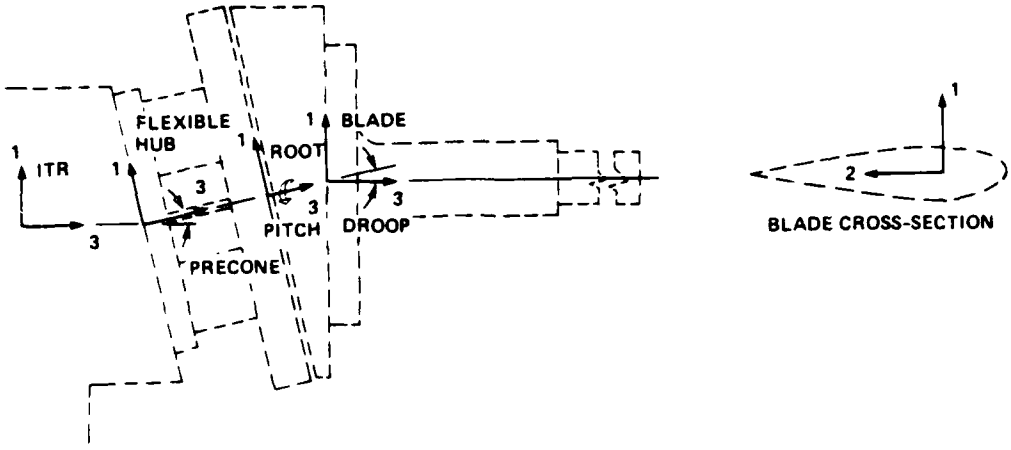

Fig. 5 Subsystem frames of reference.

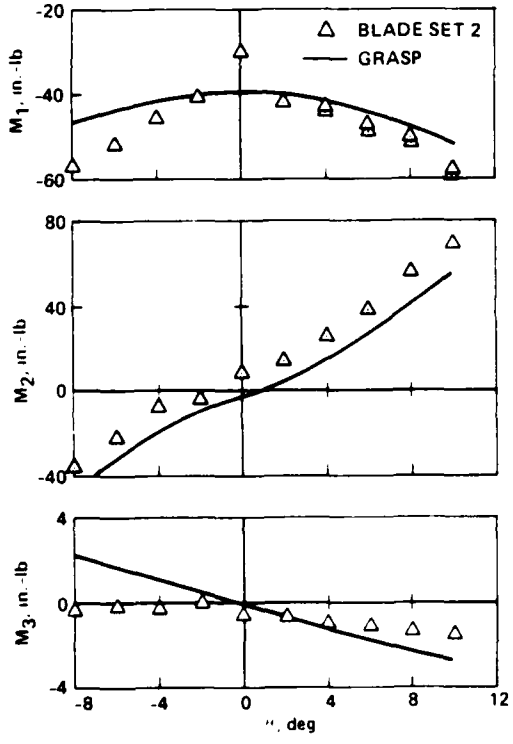

Fig. 6 Steady-state moments for Case 1 (stiff flexure, 0° precone, 0° droop).

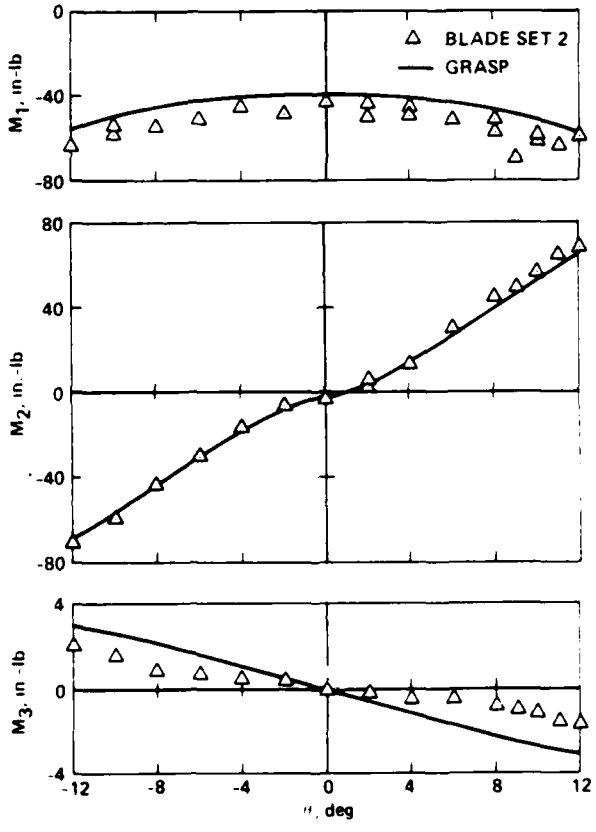

Fig. 7 Steady-state moments for Case 2 (soft flexure, 0° precone, 0° droop).

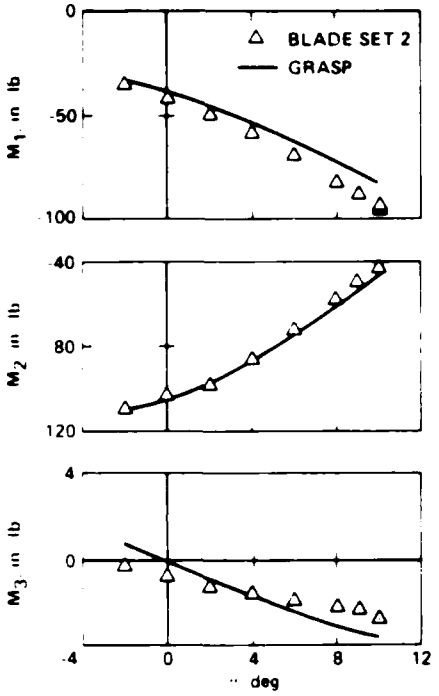

Fig. 8 Steady-state moments for Case 3 (stiff flexure, 5° precone, 0° droop).

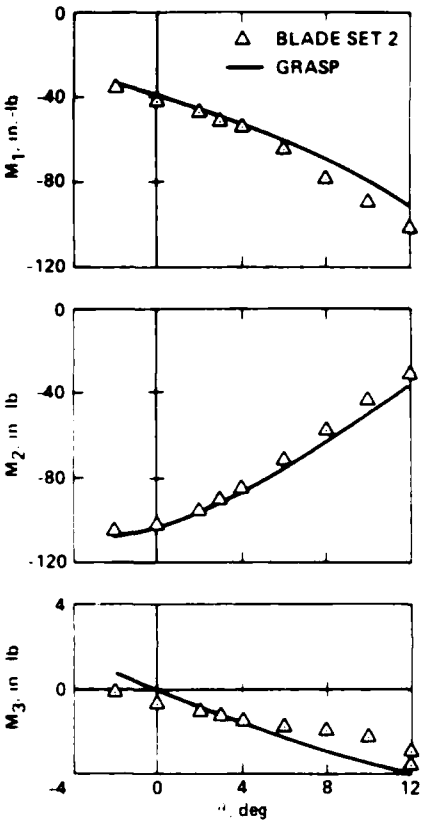

Fig. 9 Steady-state moments for Case 4 (soft flexure, 5° precone, 0° droop).

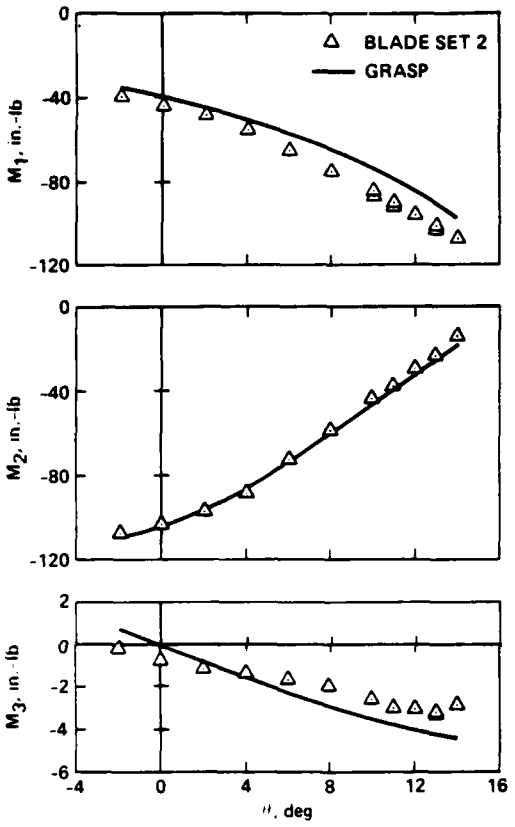

Fig. 10 Steady-state moments for Case 5 (stiff flexure, 0° precone, -5° droop).

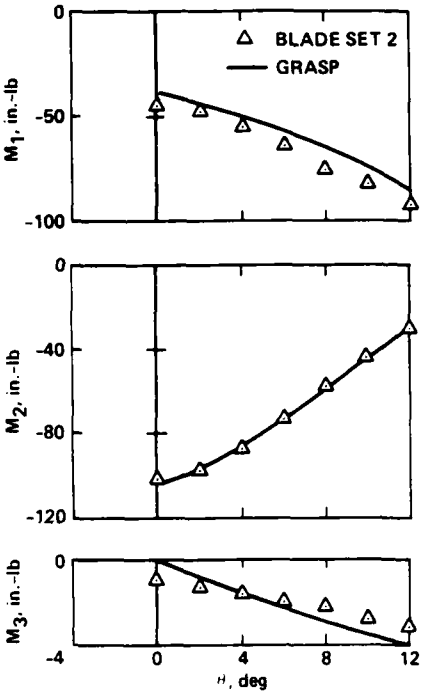

Fig. 11 Steady-state moments for Case 6 (soft flexure, 0° precone, -5° droop).

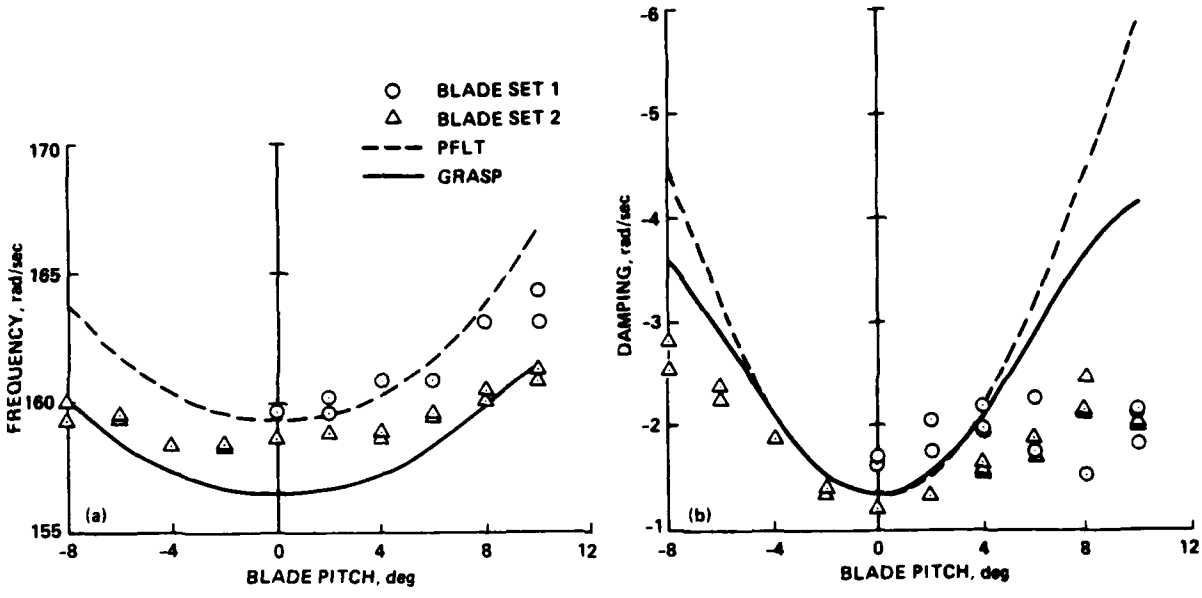

Fig. 12 Frequency and damping versus blade pitch for Case 1 (stiff flexure, 0° precone, 0° droop).

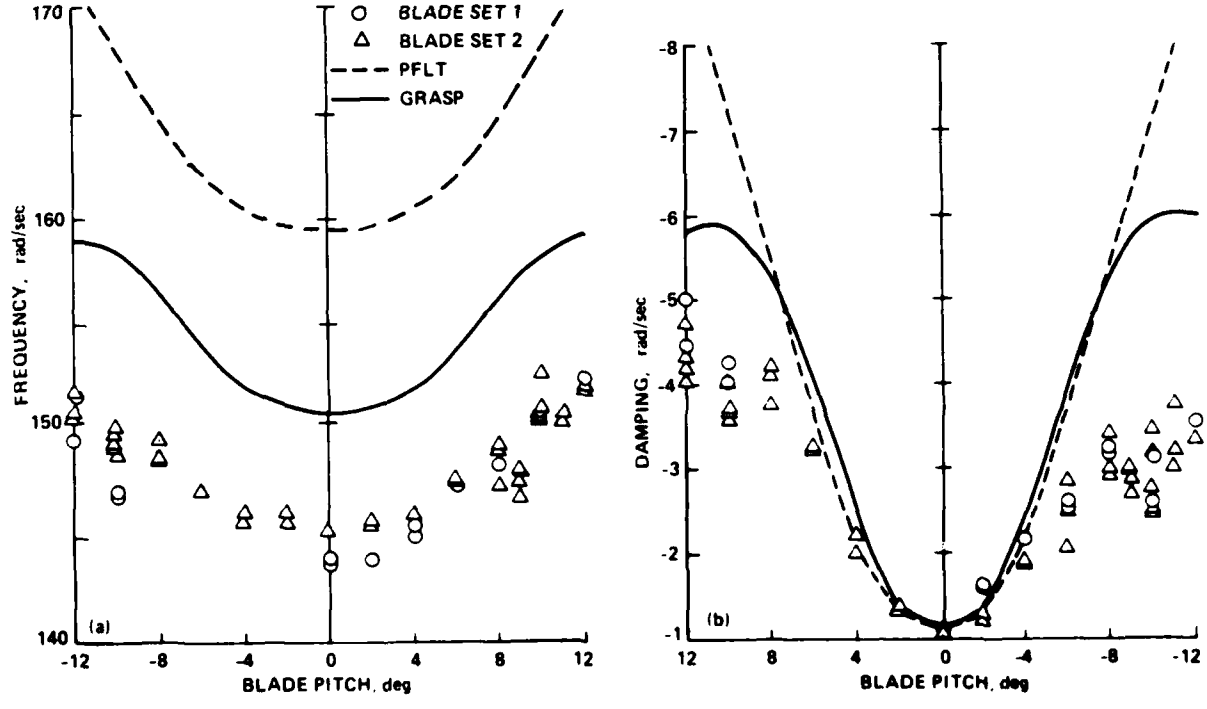

Fig. 13 Frequency and damping versus blade pitch for Case 2 (soft flexure, 0° precone, 0° droop).

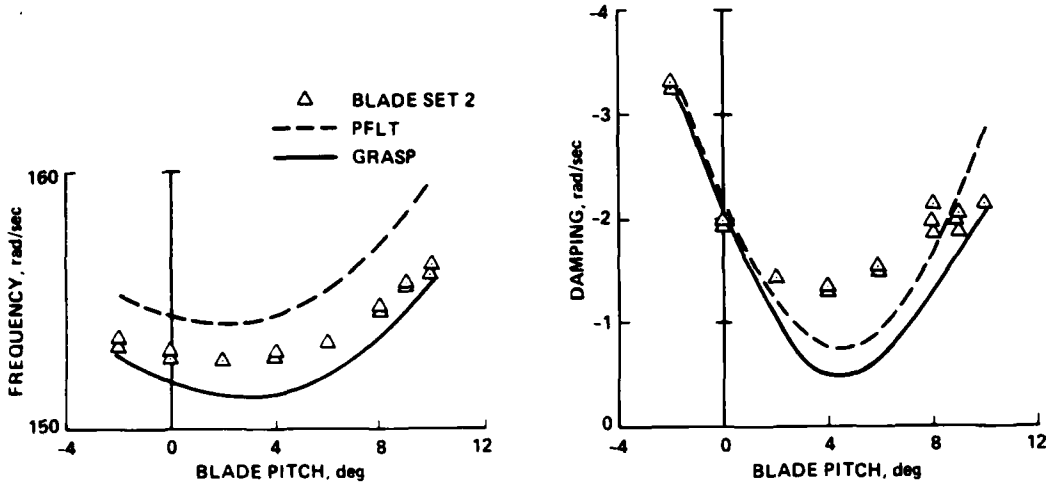

Fig. 14 Frequency and damping versus blade pitch for Case 3 (stiff flexure, 5° precone, 0° droop).

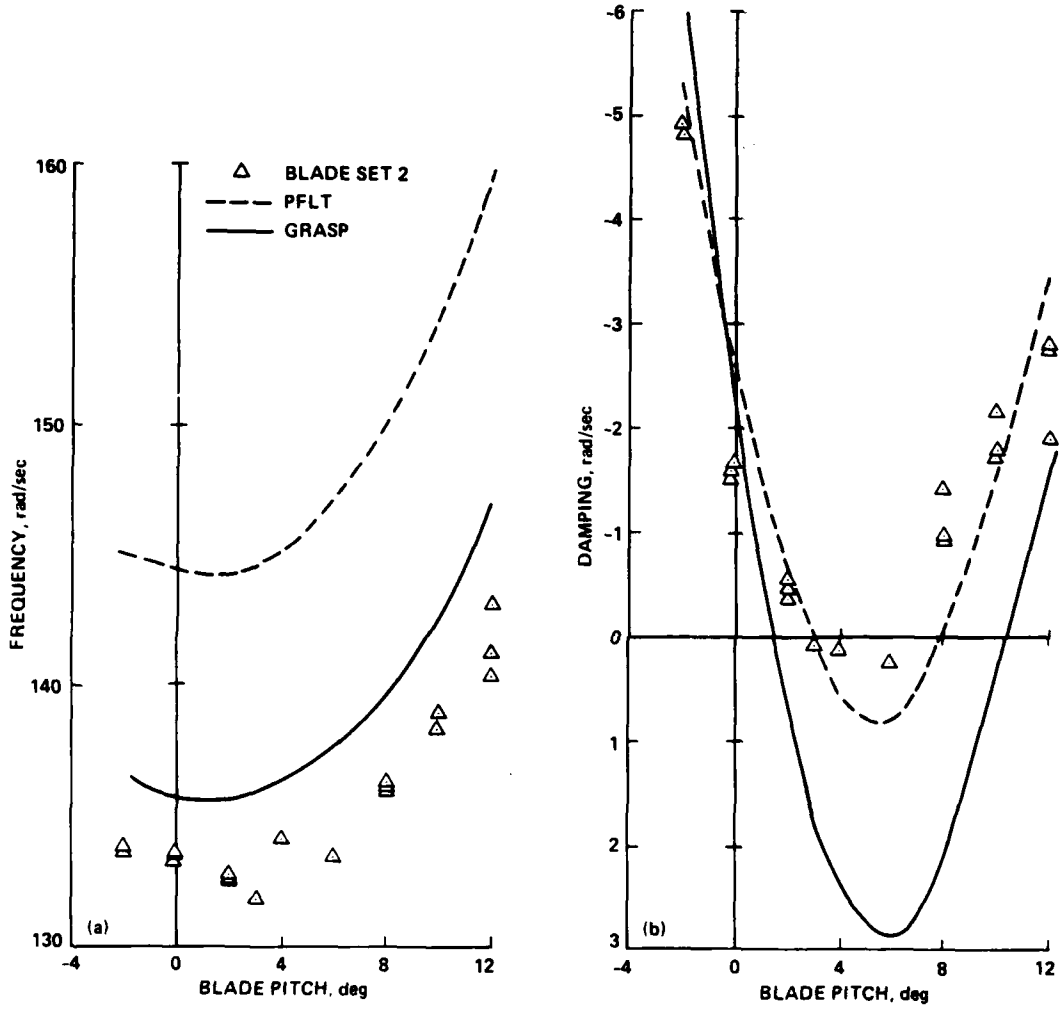

Fig. 15 Frequency and damping versus blade pitch for Case 4 (soft flexure, 5° precone, 0° droop).

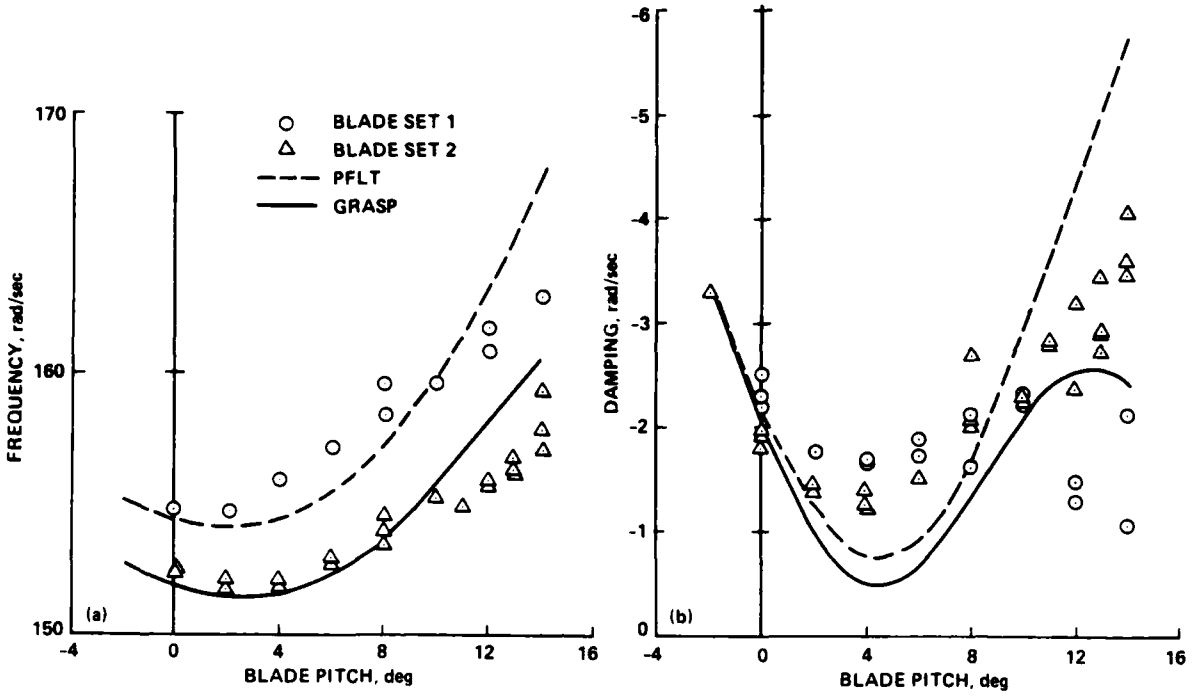

Fig. 16 Frequency and damping versus blade pitch for Case 5 (stiff flexure, 0° precone, -5° droop).

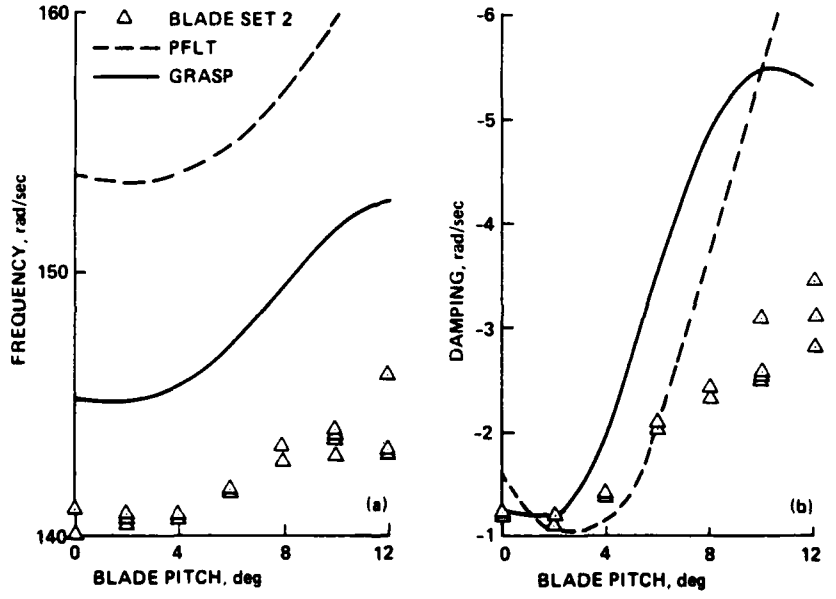

Fig. 17 Frequency and damping versus blade pitch for Case 6 (soft flexure, 0° precone, -5° droop).

END

4-87

DTIC